Proton Relay Effects in Pyridyl-Appended Hydrogenase Mimics for Proton Reduction Catalysis

Zaffaroni, R.; Dzik, W.I.; Detz, R.J.; van der Vlugt, J.I.; Reek, J.N.H.

DOI
10.1002/ejic.201900072

Publication date
2019

Document Version
Final published version

Published in
European Journal of Inorganic Chemistry

ChemPubSoc Europe

DOI: 10.1002/ejic.201900072

EurJIC European Journal of Inorganic Chemistry

Full Paper

Proton Reduction Catalysts

Proton Relay Effects in Pyridyl-Appended Hydrogenase Mimics for Proton Reduction Catalysis

Riccardo Zaffaroni,[a] Wojciech I. Dzik,[a] Remko J. Detz,[a,b] Jarl Ivar van der Vlugt,[a] and Joost N. H. Reek*[a]

Abstract: Hydrogenase enzymes are fast proton reduction catalysts, and their synthetic mimics have been widely studied in the context of solar fuel applications. The mimics are still not nearly as effective as the enzyme, as they lack crucial structural elements, including proton-relays and electron reservoirs. In this contribution we report di-iron hydrogenase model complexes of the type $Fe_2(X_4bdt)(PPy_3)_n(CO)_{6-n}$ (X = H, Cl, F; *n*= 0, 1, 2; PPy_3= *tris*(*m*-pyridyl)phosphane), featuring pyridyl-appended phosphane ligands able to act as proton relays. In organic solvents, in the presence of weak acid, the pyridyl groups remain unprotonated during the catalytic cycle; thus, proton pre-organization does not occur, and the complexes display catalytic rate constants in the order of 10^3 M^{-1} s^{-1}. Protonation of the pyridine allows for dissolution of the complexes in acidic aqueous media thus facilitating proton pre-organization, but at the same time counterbalancing the electron-donating abilities of the phosphane ligands. Catalysis thus occurs at the first reduction potential of the complexes with rate constants up to 10^8 M^{-1} s^{-1}, well beyond those observed for the natural enzymes and among the highest reported so far.

Introduction

Hydrogenases are metalloenzymes that perform the reversible proton reduction reaction at very high rates with overpotentials close to the thermodynamic limit.[1] Among the three classes of hydrogenases known, those containing a di-iron core are definitely the fastest hydrogen evolving enzymes.[2,3] In recent years this class of enzymes gained lot of interest, also in the context of renewable energy production and the transition to a carbon-neutral economy.[4] Indeed, one can envision devices, such as fuel cells or electrolyzers, based on components inspired by nature.[5,6] The active site of the enzyme, the H-cluster, is embedded in a dense protein matrix that offers protection, enables substrate preorganization and induces geometrical constraints, which forces the active site in the so-called activated rotated structure.[7] Two cofactors are essential for the high operational rates of the enzyme; i) the Fe_4S_4 cluster bounded to the distal iron, responsible for shuttling electrons into the iron-iron core and ii) the azadithiolate bridge, which acts as proton relay and thereby preorganizes the substrates (i.e. protons). The two cofactors are believed to work in synergy through proton-coupled electron transfer (PCET) steps.[8] In stark contrast herewith, current synthetic "artificial" model systems lack the protein environment. Despite mimics featuring proton relays have been reported and widely studied,[9–32] only a handful of reports describe efforts to combine the two cofactors mentioned.[33–37] Most of the mimics are of the hexacarbonyl type due to their relative ease of preparation.[34] The general drawback of this class of compounds is their low polarity, which limits their solubility and thus confines the electrochemistry studies to organic solvents. Electrochemistry studies in aqueous media with di-iron-based models are scarce and usually hampered by insolubility of the complexes. Some electrochemical data in water have been obtained using water-soluble complexes with ligands containing appropriate groups such as sulfonates,[38] by using water-soluble phosphane ligands such as PTA[39–41] (PTA = 1,3,5-triaza-7-phosphaadamantane) or by encapsulation of the apolar complexes in aqueous micellar solutions.[42,43] Recently our group reported the iron-iron model featuring a benzenedithiolate bridge and a phosphole ligand bearing two pyridine substituents shown in Scheme 1.[33] It has been shown that this particular ligand acts as dual-mode reactive platform that actively partakes in the reduction of protons, as it functions both as an electron reservoir and as proton relay, allowing for a PCET step. Furthermore, the presence of the pyridyl groups allowed for the dissolution of the complex in diluted acidic solutions, giving access to the study of this complex in aqueous media.

In this work, we set out to elucidate the exact effect of a pyridine-based proton-responsive relay, both in organic solvents and in acidic aqueous media, by decoupling this specific function from the redox-active properties of the dipyridylphosphole ligand. To this end we installed one or two tris(*meta*-

[a] *van 't Hoff Institute for Molecular Sciences, University of Amsterdam, Science Park 904, 1098 XH Amsterdam, The Netherlands*
E-mail: J.N.H.Reek@uva.nl
[b] *Current address: Energy Transition Studies, ECN.TNO, Radarweg 60, 1043 NT Amsterdam, The Netherlands*
Supporting information and ORCID(s) from the author(s) for this article are available on the WWW under https://doi.org/10.1002/ejic.201900072.

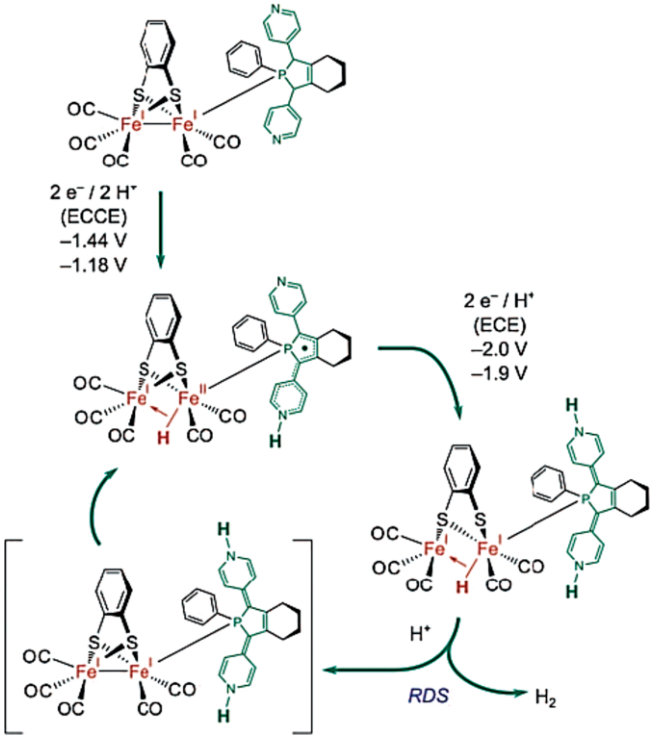

Scheme 1. Proposed mechanism of proton reduction by the di-iron phosphole derivative previously reported by our group.[33] Potentials are reported vs. Fc0/+ couple.

pyridyl)phosphane ligands onto synthetic benzenedithiolate iron-iron hydrogenase models. Introducing proton relays on the ligands allows for more freedom on the type of dithiolate bridge used. Furthermore, the number of proton relays can be easily tuned by ligand design and by the number of ligands installed on the diiron core. In addition, multiple protonation of the ligand attached to the complex allows for dissolution and study of the complexes in acidic aqueous media. As depicted in Scheme 2, the electronic properties of the catalysts are tuned by i) modification of the benzenedithiolate bridge, ii) increasing the number of trispyridylphosphane ligands coordinated to the complex and iii) protonation of these pyridyl ligands. The complexes show intricate equilibrium reactions at the electrode surface in organic solvent (dichloromethane) in the absence of acid. Nonetheless, such reactivity is not observed in the presence of weak acid; conditions relevant for catalytic purposes. It is shown that, opposed to the redox-active phosphole derivative, the mono-phosphane complexes **1a**–**3a** do not display proton-coupled electron transfer steps, which results in about two orders of magnitude lower catalytic rates in CH_2Cl_2. Regarding the bridge modification, the more electron-deficient complexes display a lower operational overpotential at the expense of a small drop in their catalytic activity. Phosphane coordination has the opposite effect; it increases catalytic rates as the complexes become more basic but also the overpotential rises as the resulting more electron-rich species are harder to reduce. The positive effect of the proton-responsive trispyridylphosphane ligands becomes evident when the catalytic activity of the various complexes is measured in diluted sulfuric acid solution; pyridyl protonation allows for dissolution of the complexes in acidic aqueous media but most importantly it counterbalances the electron-donating properties of the phosphanes and preorganizes protons around the di-iron center, allowing for unprecedented proton reduction rates that reach values up to 10^8 M^{-1} s^{-1}, far beyond rates displayed by the hydrogenase enzymes.

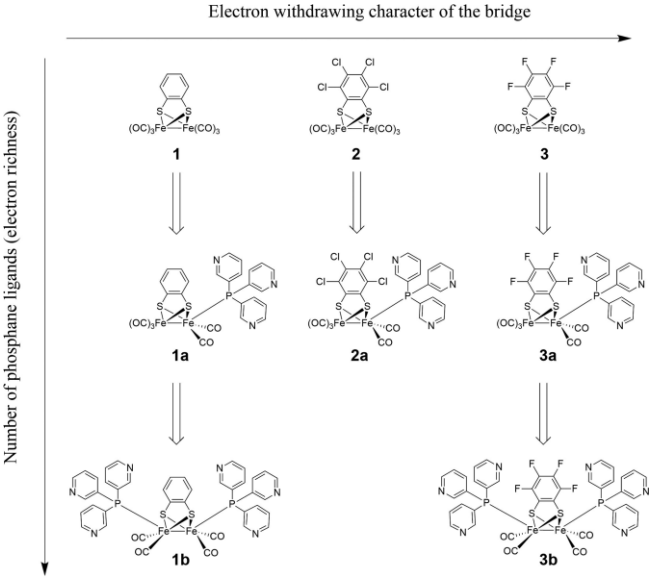

Scheme 2. Overview of the complexes described.

Results

We first describe the synthesis and characterization of the bdt-derived complexes **1–3** with varying equivalents of P(*m*-Py)$_3$ ligand incorporated. Next, the electrochemical data in dichloromethane (DCM) in the absence of acid is presented, showing the redox behavior of the complexes. The subsequent section describes in detail the follow-up reactivity of the complexes after the first electron transfer. Next, the catalytic behavior of the complexes is described. Experiments performed in dichloromethane in the presence of a weak acid are presented first, followed by their behavior in the presence of stoichiometric amounts of strong acid. Finally, the catalytic studies of the P(*m*-Py)$_3$ containing complexes in acidic aqueous media are presented. In the discussion section, the results will be discussed in a broader context.

Synthesis and Characterization

Tetrachlorobenzenedithiol[44,45] and tetrafluorobenzenedithiol[46] were prepared according to modified literature procedures. The di-iron dithiolate hexacarbonyl complexes **1–3** were prepared by reaction of the corresponding substituted benzenedithiol with stoichiometric amounts of the iron precursor $Fe_3(CO)_{12}$ in refluxing toluene. The hexacarbonyl complexes have been converted into the corresponding mono-*tris*-(*m*-pyridyl)phosphane derivatives **1a**–**3a** by treatment with the decarbonylating agent trimethylamine *N*-oxide in the presence

of one equivalent of P(*m*-Py)$_3$. Purification of the complexes was achieved by column chromatography. The two bis-phosphane complexes **1b** and **3b** were prepared by refluxing a toluene solution of the parent hexacarbonyl compounds in the presence of two equivalents of P(*m*-Py)$_3$. Isolation of the desired species was achieved by recrystallization from DCM/hexane mixtures.

Complexes **1** and **2** were reported and extensively characterized before.[47,48] The novel tetrafluoro-benzenedithiolate hexacarbonyl complex **3**, the mono- (**1a**–**3a**) and bis-phosphane derivatives (**1b** and **3b**) have been characterized thoroughly by multinuclear NMR and FT-IR spectroscopy, high resolution mass spectrometry, cyclic voltammetry and X-ray crystallography. For the phosphane containing compounds, a second set of measurements has been carried out in diluted sulfuric acid to evaluate the stability of these species under aqueous acidic conditions. The relevant analytical data for the complexes are compiled in the supporting information.

Figure 1 shows the solid state molecular structures of the complexes. They display the typical butterfly conformation of the di-iron core, with each Fe being in a distorted octahedral geometry. The phosphane ligands are always located in the apical position, in agreement with literature data reported on benzenedithiolate analogs.[49–51]

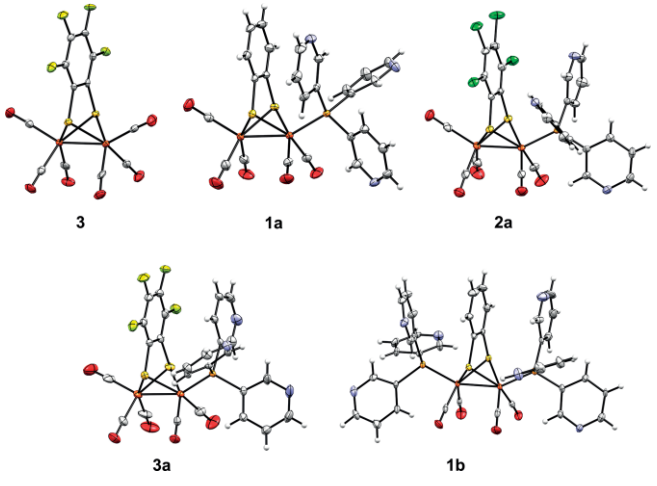

Figure 1. X-ray crystal structures of **3** [$Fe_2(F_4bdt)(CO)_6$] (CCDC 1848258), **1a** [$Fe_2(bdt)(CO)_5PPy_3$] (CCDC 1848256), **2a** [$Fe_2(Cl_4bdt)(CO)_5PPy_3$] (CCDC 1848257), **3a** [$Fe_2(F_4bdt)(CO)_5PPy_3$] (CCDC 1848259), and **1b** [$Fe_2(bdt)(CO)_4(PPy_3)_2$] (CCDC 1848260). Thermal ellipsoids are set at 50 % probability.

Analysis of the crystallographic data suggests negligible structural differences among complexes with the same number of CO ligands. Furthermore, the crystallographic data show that the complexes are rather similar in terms of bond lengths, even when a different number of phosphane ligands are coordinated. On the other hand, the IR data, particularly in the CO region, show that the electronic properties of the complexes are significantly different, following the expected trend, in line with the electron-withdrawing properties of the dithiolate bridge ($\Delta\nu$ +8 cm^{-1} from **1a** to the more electron deficient **3a**) and the electron-donating properties of the phosphanes ($\Delta\nu$ −25 cm^{-1} per phosphane ligand). The complexes were found to be oxygen tolerant in the solid state, but decomposition was observed when their aerobic solutions were exposed to either light or acetonitrile.

Cyclic Voltammetry in CH_2Cl_2

The voltammetric responses for **1** and **2** have already been thoroughly investigated under a wide variety of conditions.[43,48,52–54] The cyclic voltammogram of the tetrafluorobenzenedithiolate derivative **3** in DCM solution in absence of acid is shown in Figure 2, together with those obtained for **1** and **2**. Complex **3** displays a reversible single wave event at −1.27 V vs. Fc/Fc$^+$, which is almost identical to the redox potential for **2**. The electrochemical event is a two-electron process with potential inversion, as determined by isopoint analysis[55] and bulk electrolysis, similarly to what is known for **1** and **2**. Switching from the benzenedithiolate derivative **1** (electronegativity of H substituent: 2.1) to the more electron-withdrawing tetrachloro-derivative **2** (electronegativity of Cl substituent: 3.0) lowers the reduction potential of the complex by about 120 mV. Increasing the electronegativity of the benzene ring substituents even more with the tetrafluoro complex **3** (electronegativity of F substituent: 4.0), lowers the reduction potential by a mere 8 mV. This small change is in agreement with the predicted properties using the Hammet parameters for Cl and F substituents.

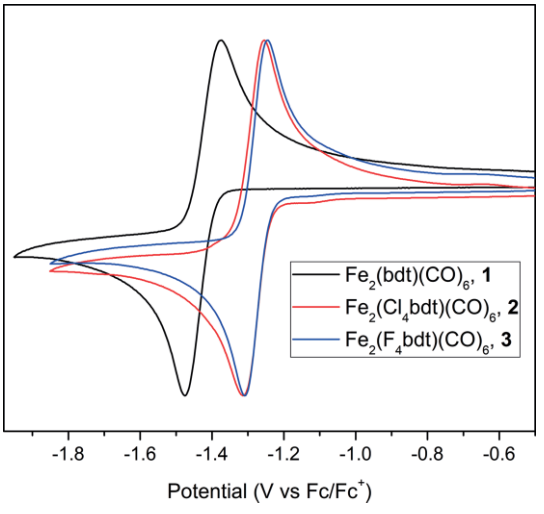

Figure 2. Comparison of voltammograms for complexes **1–3** in DCM solution at 20 mV/s.

Preliminary experiments in the presence of weak acid showed similar behavior for **3** and the other two complexes of the series, therefore further detailed analysis and proton reduction data of the fluoro-based complex are omitted. The mono-phosphane complexes **1a**–**3a** show single electrochemical reduction events at −1.58 and −1.47 V vs. Fc/Fc$^+$ that appear quasi-reversible, with the back-oxidation trace showing two distinct peaks (Figure 3). Unlike the parent hexacarbonyls, the mono-phosphane derivatives undergo a one-electron reduction, as established by analysis of the semi-integrative convolution plots for the complexes in the presence of equimolar

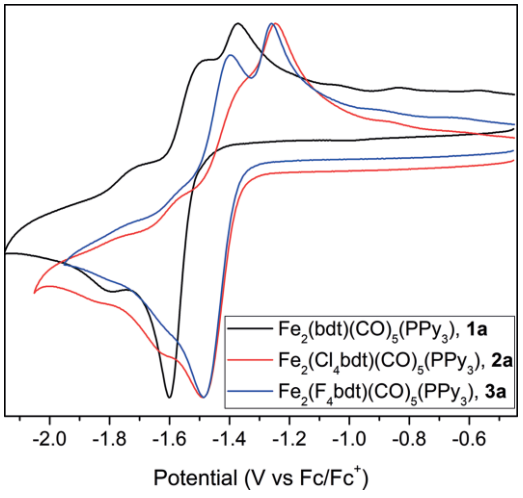

Figure 3. Cyclic voltammograms of the mono-phosphane derivatives **1a**–**3a** in DCM solution at 20 mV/s.

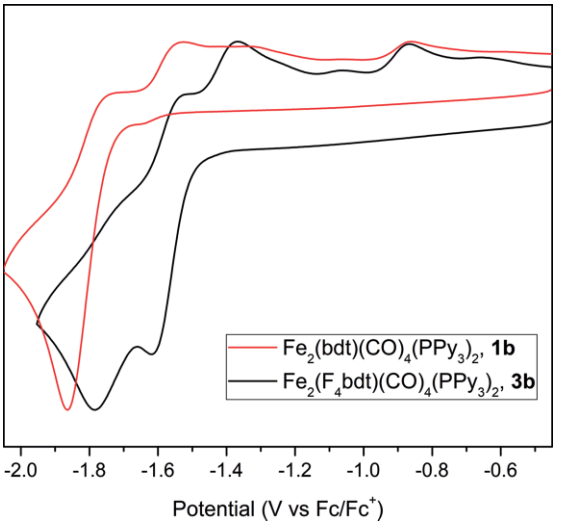

Figure 4. Cyclic voltammograms of the bis-phosphane derivatives **1b** and **3b** in DCM solution at 100 mV/s.

amounts of ferrocene (Figure S38). Even though it is known that this method introduces approximations and errors due to the lack of knowledge of the diffusion coefficients of the species, it gives a reasonable indication on the number of electrons involved in the process.[56] We note that bulk electrolysis, which is typically a more accurate method to determine the number of electrons involved in a given process, is problematic in this case due to the follow-up reactivity of the complexes, as indicated by the second minor reduction event, about 150–200 mV after the primary reduction, a topic described in the next section. The bis-phosphane complex **1b** displays a single non-reversible reduction peak at –1.86 V vs. Fc/Fc^+ while the tetrafluoro-derivative **3b** shows two non-reversible events at –1.56 V and –1.78 V (Figure 4). Interestingly, the back-oxidation traces for both compounds show overlapping peaks at –0.9 V that are attributed to a common decomposition pathway of dithiolate dissociation. Semi-integrative convolution plots obtained from an equimolar solution of ferrocene and complex **1b** or **3b** indicate a one-electron process for the first reduction event of either complex (Figure S38 and Figure S39).

The single reduction event observed for complex **1b** splits into two different events at relatively high scan rates (> 1 V/s). On the other hand, the two reduction events for complex **3b** converge into one peak at relatively low scan rates (< 20 mV/s). This phenomenon is tentatively attributed to a follow-up rearrangement of the complexes, e.g. apical to basal phosphane rotation, loss of phosphane ligand or iron–sulfur bond breaking upon reduction.[51] If sufficient time is allowed after the mono-reduction (low scan rates), the rearrangement can take place and the newly generated species cannot be reduced again. On the contrary, when the rearrangement does not take place (high scan rates) the mono-reduced complexes can be reduced a second time. In order to understand this scan-rate dependency and the origin of the minor reduction events observed for the mono-phosphane derivatives, we investigated in more detail the reactivity of the phosphane-substituted complexes upon mono-reduction, by cycling voltammetric experiments in non-stirred solutions.

Follow-Up Reactivity upon First Reduction

For complexes **1a**–**3a**, the second minor reduction event, about 150–200 mV after the primary reduction, discussed in the previous section, becomes more pronounced at low scan rates. This suggests a time dependent follow up reaction triggered by the electrochemical reduction. The redox potentials of the evolving species are found to be consistent with those of the bis-substituted complexes **1b**–**3b**, suggesting that ligand exchange might take place upon reduction. Such reactivity has been suggested for the mono-substituted bis-diphenylphosphinomethane (dppm) di-iron complex; its electrochemical reduction induces a disproportionation reaction associated with intramolecular rearrangement to the chelating diphosphane derivative following CO dissociation.[57] Figure 5 shows that for complex **1a**, when consecutive voltammograms are recorded without refreshing the solution at the working electrode, a third reduction event appears at –1.50 V, which coincides with a redox potential of hexacarbonyl species **1**, as shown by a spiking experiment with an authentic sample of **1** (Figure S40). This observation supports the occurrence of a disproportionation reaction associated with ligand exchange, triggered by the mono-reduction of the mono-phosphane complexes (Figure 6, top). A similar process is known for mono-substituted propanedithiolate di-iron complexes.[58,59] Validation of this hypothesis came from spectroelectrochemistry coupled with FT-IR spectroscopy, which clearly reveals the simultaneous appearance of two distinct species upon reduction of the mono-phosphane derivatives. One species was found to be identical to the neutral bis-phosphane complexes while the other can be ascribed to the doubly reduced hexacarbonyl parent complexes. Figure 6 (bottom) displays an overlay of the IR-spectroelectrochemistry data for the benzenedithiolate series of complexes **1**, **1a** and **1b**. Although electrochemical conversion of similar hexacarbonyl species into the mono- and bis-phosphane complexes has been reported, the process which generates the di-anion of the hexacarbonyl parent complex has never been observed for benzenedithiolate di-iron complexes.[60] Furthermore, we sus-

pected the existence of intricate equilibrium reactions at the electrode surface as during the cycling experiment described in Figure 5, a steady state is quickly reached after a couple of cycles and further accumulation of the hexacarbonyl and bis-phosphane complexes is not observed.

A separate cycling experiment using an equimolar solution of **1** and **1a** showed no change of the voltammogram upon repeated voltammetric cycles, suggesting that the equilibrium was already established (Figure S41). However, if additional phosphane ligand is added to the solution (about 25 equivalents), both signals for **1** and **1a** gradually decrease while that of **1b** increases, being the predominant species at the electrode surface (Figure S42). Although about 12 equivalents of free phosphane ligand per di-iron complex are present in solution, a steady state is quickly reached. Since clear accumulation of **1b** at the electrode is not observed, the collected experiments suggest that all complexes could undergo further rearrangement upon reduction. In line with these experiments, Figure 7 shows a cycling experiment starting with a solution of complex **1b** which shows already at the second cycle the appearance of significant amounts of the mono-phosphane derivative **1a**. In this case, a disproportionation event can be excluded since the triply substituted di-iron complex is not observed. To the best

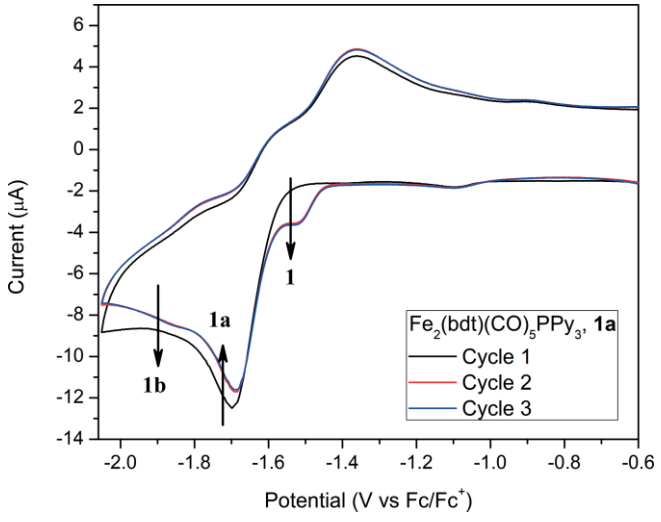

Figure 5. Repeated cyclic voltammograms for **1a**, showing the appearance of **1** around –1.50V, at the second cycle; 100 mV/s.

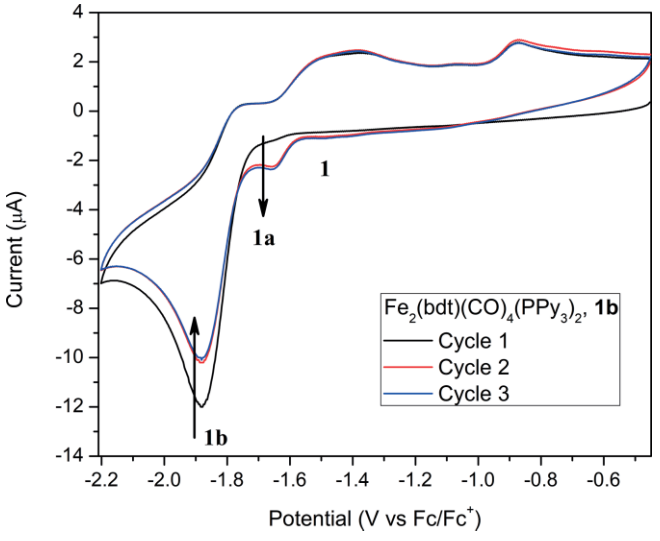

Figure 7. Repeated cyclic voltammograms for **1b**, showing the appearance of **1** and **1a** at the second cycle; 100 mV/s.

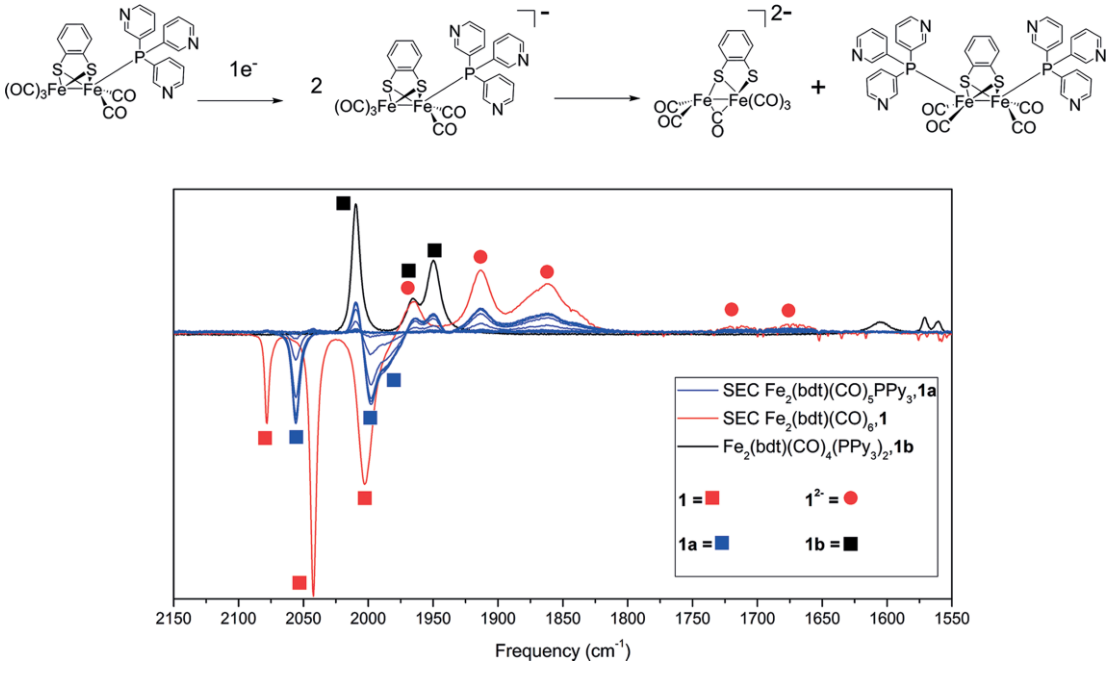

Figure 6. Top: reactivity of mono-phosphane derivative **1a** upon mono-reduction. Complexes **2a** and **3a** behave similarly. Bottom: FT-IR spectroelectrochemistry data. Black: IR of **1b**. Red: spectroelectrochemistry measurement for **1** after its reduction, showing the bleaching of **1** and the appearance of $\mathbf{1}^{2-}$. Blue: spectroelectrochemistry measurement for **1a** showing its bleaching and simultaneous appearance of $\mathbf{1}^{2-}$ and **1b**.

of our knowledge, no examples of (isolated) benzenedithiolate tris-phosphane di-iron complexes have been reported. It is noted that in order to generate **1a** from the reduction of **1b** an additional CO ligand is needed, likely coming from the decomposition of a second molecule of **1b**. The hexacarbonyl derivative **1** is also detected at the second cycle, albeit in lower amounts.

Lastly, we measured an equimolar solution of complex **1** and **1b**. At the first cycle only the two expected complexes are detected, indicating that there is no fast reaction between the doubly reduced hexacarbonyl ($\mathbf{1}^{2-}$) and **1b** in its neutral form. Instead, significant amounts of **1a** are present at the electrode after the second consecutive cycle. Interestingly both the intensity of **1** and **1b** are now lower, suggesting that **1a** is generated independently from the mono-reduction of **1b** and from the reaction of $\mathbf{1}^{2-}$ with the free phosphane liberated in solution after reduction of **1b** (Figure S43). Table 1 summarizes the described reactivity during the electrochemical reduction of complexes **1**, **1a** and **1b**. Interestingly, several literature reports on phosphane substituted benzenedithiolate complexes show similar voltammograms, indicating that such intricate reactivity upon reduction might be a more general phenomenon for such type of compounds.[51,61]

Table 1. Summary of the reactivity observed during electrochemical reduction of complexes **1**, **1a**, and **1b**. Schemes are compiled in Table S6.

	Starting solution	Additional species detected at 2nd cycle
1	**1** + PPy_3	**1a** + **1b**
2	**1a**	**1** + **1b**
3	**1b**	**1** + **1a**
4	**1a** + **1**	–
5	**1** + **1a** + PPy_3	**1b**
6	**1**+**1b**	**1a**

Proton Reduction from Weak Acid in CH_2Cl_2

When complex **1a** is studied using cyclic voltammetry in CH_2Cl_2 in the presence of the weak acid $HNEt_3PF_6$ – this acid is not strong enough to protonate either the Fe–Fe bond of the neutral species or the basic nitrogen of the pyridine ligands – the first reduction peak at –1.58 V becomes completely irreversible and a new oxidation peaks appear around –0.5 V. This behavior is consistent with the reduction of the complex, followed by protonation of the Fe–Fe bond to yield a bridging hydride. When the potential window is increased to more reductive potentials, a new peak appears around –1.90 V. Figure 8 shows that this peak increases in intensity with increasing aliquots of acid, revealing the catalytic nature of the process. The behavior of complex **2a** and **3a** are very similar. Combining the information obtained in the absence of acid for the first redox event with the new information in the presence of acid, the overall proton reduction mechanism by which complexes **1a**–**3a** operate can be summarized as an ECEC type. This mechanism has been proposed for similar complexes,[51] indication that the pyridyl groups do not partake at the catalytic mechanism as they remain in the unprotonated state during the catalytic cycle. As catalytic plateau current were not reached, foot-of-the-wave (FotW) analysis[62] was employed to deduce the proton reduction rate constant and related turnover frequency for the complexes (Figure S47). This analysis revealed a k_{cat} in the order of 2×10^3 M^{-1} s^{-1}. Table 2 summarizes the relevant kinetic data for complexes **1a**–**3a.** Complexes **1b** or **3b** show about 100 mV anodic shift of their reduction potential when in the presence of $HNEt_3PF_6$, Figure 9. Even though the current at the first reduction peak increases slightly, the semi-integral plot and comparison with the redox waves from equimolar amounts of ferrocene present in solution indicate that this is still a one-electron process. Since the weak acid used protonates neither the Fe–Fe bond nor the pyridyl ligands, the large potential shift observed upon reduction in the presence of weak acid can be attributed to a concerted proton-coupled electron transfer step.[63,64]

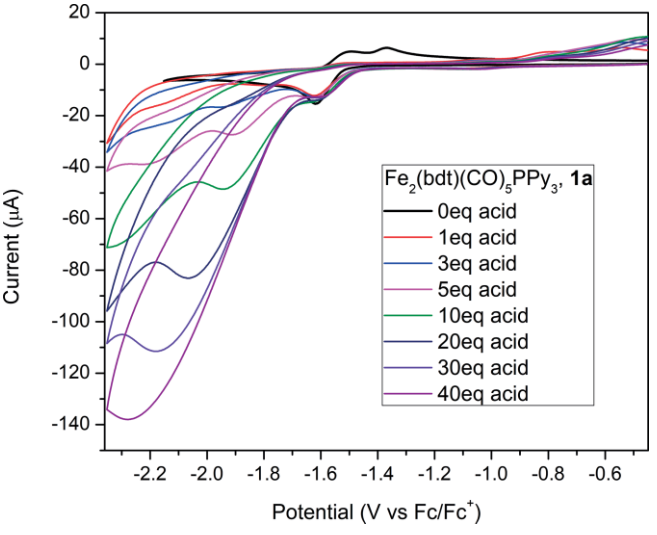

Figure 8. Voltammetric response of **1a** in the presence of increasing amounts of acid ($HNEt_3PF_6$).

Table 2. Catalytic parameters for complexes **1a**–**3a** **1b** and **3b** in DCM solution in the presence of weak acid ($HNEt_3PF_6$). TOF_{max} values are extrapolated for a 1 M concentration of acid.

	$Fe_2(bdt)(CO)_5PPy_3$ **1a**	$Fe_2(Cl_4bdt)(CO)_5PPy_3$ **2a**	$Fe_2(F_4bdt)(CO)_5PPy_3$ **3a**	$Fe_2(bdt)(CO)_4(PPy_3)_2$ **1b**	$Fe_2(F_4bdt)(CO)_4(PPy_3)_2$ **3b**
k_{cat} (M^{-1} s^{-1})	2.77×10^3	2.36×10^3	1.96×10^3	3.65×10^3	2.50×10^3
Catalytic $E_{1/2}$ potential (V vs. Fc/Fc^+)	–1.95	–1.90	–1.85	–2.13	–2.05
η [V]	0.68	0.63	0.58	0.86	0.78
TOF_{max} (s^{-1})	2.77×10^3	2.36×10^3	1.96×10^3	3.65×10^3	2.50×10^3

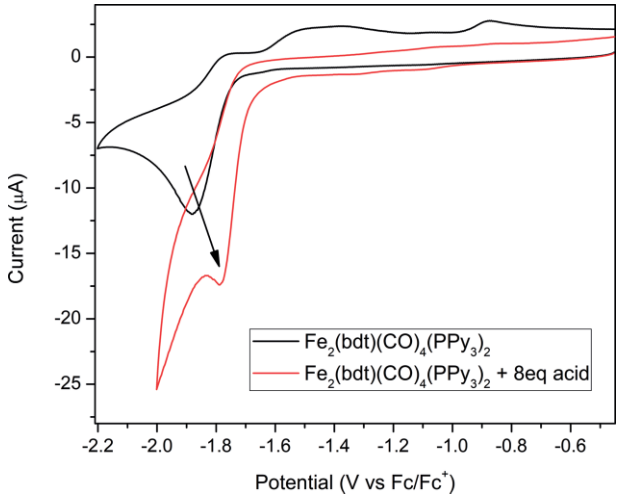

Figure 9. Voltammogram of **1b** in absence of acid (black line) and in the presence of 8 equivalents of weak acid ($HNEt_3PF_6$) showing a 100 mV potential shift indicating a PCET. Proton reduction catalysis onset at –1.85 V.

Complexes **1a**–**3a**. Complexes **1b** or **3b** show about 100 mV anodic shift of their reduction potential when in the presence of $HNEt_3PF_6$, Figure 9. Although the current at the first reduction peak increases slightly, the semi-integral plot and comparison with the redox waves from equimolar amounts of ferrocene present in solution indicate that this is still a one-electron process. Since the weak acid used protonates neither the Fe–Fe bond nor the pyridyl ligands, the large potential shift observed upon reduction in the presence of weak acid can be attributed to a concerted proton-coupled electron transfer step.[63,64]

Increasing the potential window to more reductive potentials reveals the appearance of a new catalytic wave with an onset potential at –1.85 V and a peak potential at about –2.05 V (Figure S44). Similar to that for the mono-phosphane complexes, the catalytic mechanism for the bis-phosphane complexes can be summarized as an ECEC mechanism where the first EC is a concerted step. Proton reduction rates for **1b** and **3b** are reported in Table 2, deduced from FotW analysis (Figure S48); the catalytic rate constants for the bis-phosphane complexes were found to be slightly higher than for the mono-phosphane counterparts, with k_{cat} in the order of about 3×10^3 M^{-1} s^{-1}. Despite the initial concerted step, also for the bis-phosphane complexes the presence of proton relays does not provide proton preorganization for catalysis as suggested by the catalytic mechanism and rate constants.

Interestingly, the presence of the weak acid does not allow for the side reactivity described in the previous section. Comparison of the cyclic voltammograms for the hexacarbonyl species to those obtained for complexes **1a**–**3a** in the presence of the weak acid indicate that in the presence of up to 4 equivalents of substrate, disproportionation still happens as a minor event. In the presence of higher amounts of acid, disproportionation is not observed, indicating that protonation and disproportionation proceed with roughly similar rates. Analogous comparisons for complexes **1b** and **3b** indicate that the bis-phosphane complexes behave differently. Even with small amounts of weak acid, any side reactivity is completely suppressed, possibly due to the inherently fast proton coupled electron transfer step involved in the mechanism. In addition, the main catalytic proton reduction catalysis for the bis-phosphane complexes happens at potentials about 200 mV cathodically shifted compared to their mono-substituted counterparts, in agreement with the higher electron density at the di-iron center. Regarding bridge substitution, more electron deficient complexes show lower proton reduction potentials, therefore lower overpotentials but at the expenses of decreased catalytic rates.

Study of the Complexes in CH_2Cl_2 with Strong Acid

Next, we studied proton reduction catalysis in the presence of HBF_4, a strong acid. This acid is sufficiently strong to protonate either the pyridyl groups at the phosphane ligand or the iron-iron bond. However, a reaction with a stoichiometric amount of such acid did not lead to a bridging hydride species, as indicated by ^1H NMR spectroscopy. This suggests that the pK_a of the trispyridylphosphane ligand is lower than that of the di-iron fragment. Addition of one equivalent of strong acid to **1a** causes the first reduction potential to shift anodically by about 230 mV (Figure 10). A second reduction event is also present at potentials similar to that of the first reduction of the complex in absence of acid. Addition of a second equivalent of HBF_4 causes the first reduction potential to shift by an additional 150 mV. Exhaustive investigation is hampered by precipitation of the poorly soluble doubly protonated complex. For complex **1b** a similar trend is observed, with an anodic potential shift of about 520 mV upon addition of one equivalent of acid (Figure S45). As this complex showed PCET in the presence of weak acid, this shift is most likely due to a combination of ligand protonation and PCET. Detailed proof is hard to obtain due to the poor solubility of the mono-protonated species. Nonetheless, these experiments indicate that ligand protonation has the beneficial effect of lowering the redox potential of the first electron transfer to milder values.

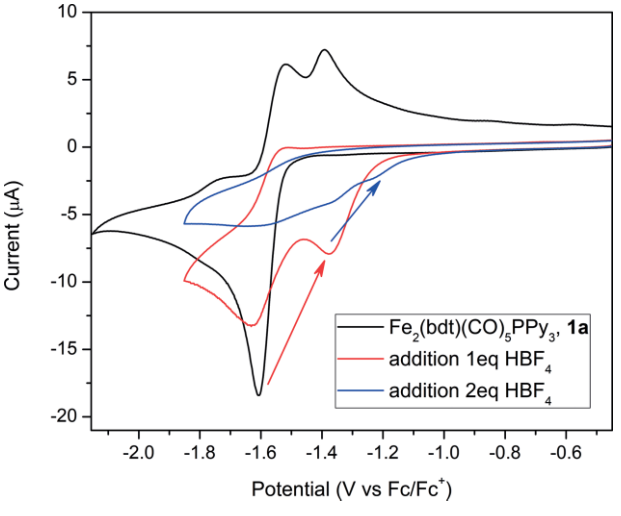

Figure 10. Voltammetric response of complex **1a** in the absence of acid or with 1 and 2 equivalents of HBF_4. After addition of the second equivalent of acid, most of the complex precipitates from solution.

Catalysis in Diluted H_2SO_4

In contrast to the protonated species in dichloromethane, complexes **1a**–**3a**, **1b** and **3b** dissolve well in acidic aqueous solutions. This allowed us to study electrocatalytic proton reduction at a glassy carbon working electrode in acidic aqueous media. The complexes show very high activity at typical 1 mM concentration; therefore, the experiments were performed at 25 μM catalyst concentration in 0.5 M H_2SO_4 solution. The analytical data presented in the supporting information demonstrate the great stability of the complexes under such harsh acidic conditions, provided that the combination of light and oxygen is avoided. Furthermore, ^{1}H NMR and FT-IR spectroscopy also indicate that in diluted sulfuric acid only protonation of the pyridyl ligands occurs, while the di-iron bond stays intact. Under the described conditions, complexes **1a**–**3a** show scan speed-independent plateau currents at –1.0 V vs. NHE, similar to their first reduction in organic solvents and catalytic proton reduction thus occurs at the first redox event. The S-shaped voltammograms obtained for **1a** (Figure 11) indicate that electrocatalysis occurs under pure kinetic control with negligible depletion of substrate. Application of FotW analysis provides calculated reaction rates values k_{cat} as high as 10^7 M^{-1} s^{-1} for **1a** and 9×10^5 M^{-1} s^{-1} for **3a** (Figure S49).[62]

Complexes **1b** and **3b** are also extremely active under these conditions, as their 25 μM solutions in 0.5 M H_2SO_4 display a diffusion-limited shape of the catalytic curve (Figure 12). The shape of the voltammograms suggests a rapid depletion of substrate, which is a first indication that these complexes are faster catalysts than their mono-substituted analogs. In these experiments the catalytic rates were deduced by FotW analysis and found to reach unprecedented values in the order of 10^8 M^{-1} s^{-1} (Figure S50). Table 3 summarizes the relevant data for the complexes in acidic aqueous environment. Protonation of the pyridyl groups offers effective substrate preorganization around the catalytic centers as indicated by the high catalytic rates obtained.

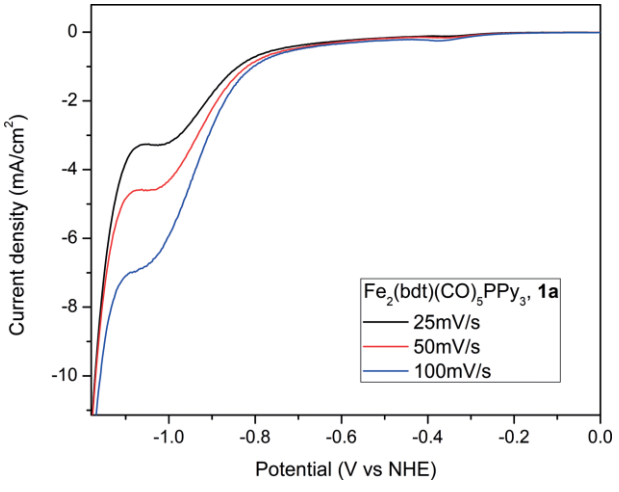

Figure 11. Catalytic voltammetric response of a 25 μM solution of mono-phosphane **1a** in 0.5 M H_2SO_4 at different scan speeds.

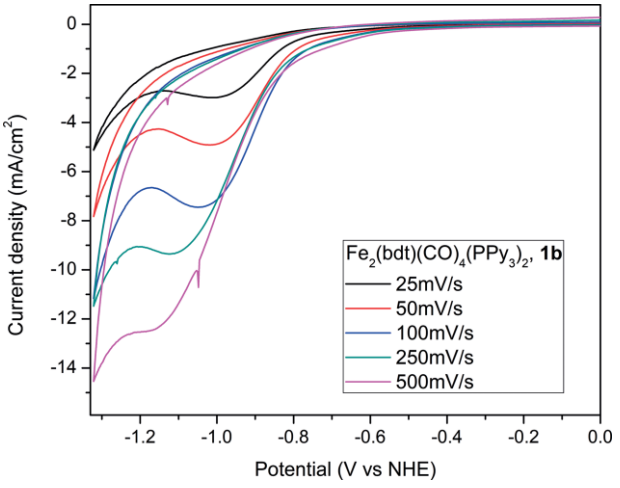

Figure 12. Catalytic voltammetric response of a 25 μM solution of bis-phosphane **1b** in 0.5 M H_2SO_4 at different scan speeds.

Discussion

In the absence of acid, the bdt-derived complexes display a rich variety of equilibrium reactions upon reduction, including interconversion of the complexes with higher degree of CO-substitution, disproportionation and even decomposition pathways. Although these undesired reactions raise questions on the stability of the complexes, it is important to address the relevance of such reactivity under catalytic conditions i.e. in the presence of protons. Our experiments indicate that for the mono-phosphane derivatives **1a**–**3a** protonation and disproportionation have roughly similar rates. As such, under catalytic conditions in the presence of several equivalents of acid, disproportionation is not observed. For complexes **1b** and **3b** any side reactivity is completely suppressed even with small amounts of weak acid, likely due to the inherently fast proton coupled electron transfer step involved in the mechanism. This underlines the importance to study the complexes under a diverse set of conditions.

Table 3. Catalytic parameters for complexes **1a**–**3a**, **1b** and **3b** in 0.5 M H_2SO_4 solution. TOF_{max} are for 1 M concentration of protons substrate; 0.5 M H_2SO_4 solution.

	$Fe_2(bdt)(CO)_5PPy_3$ **1a**	$Fe_2(Cl_4bdt)(CO)_5PPy_3$ **2a**	$Fe_2(F_4bdt)(CO)_5PPy_3$ **3a**	$Fe_2(bdt)(CO)_4(PPy_3)_2$ **1b**	$Fe_2(F_4bdt)(CO)_4(PPy_3)_2$ **3b**
k_{cat} (M^{-1} s^{-1})	1.8×10^7	9.2×10^5	5.4×10^5	2.7×10^8	4.0×10^6
Catalytic $E_{1/2}$ potential (V vs. NHE)	–0.90	–0.86	–0.85	–0.97	–0.92
η [V]	0.82	0.78	0.77	0.89	0.84
TOF_{max} (s^{-1})	1.8×10^7	9.2×10^5	5.4×10^5	2.7×10^8	4.0×10^6

The electrochemical data presented for the reduction of the complexes **1–3**, **1a**–**3a**, **1b** and **3b**, either in dichloromethane and in diluted H_2SO_4 solution, follow a general trend that is in line with the FT-IR data. The average CO frequency of the three most intense carbonyl signals is often used as an indicator of the electron density at the di-iron core. A more electron-withdrawing bridge results in a minor shift of the CO bands to higher wavenumbers e.g. from **1** to **3** the average shift is about 8 cm^{-1}. A higher number of phosphane ligands results in a major shift to lower wavenumbers, e.g. from **1** to **1b** the average shift is about 60 cm^{-1}, in line with literature precedents.[48–50] The average CO shift also correlates well with the reduction potential of the complexes. Figure 13 summarizes this data for all the complexes presented here; increasing the electron-withdrawing character of the bridge shifts the reduction potential of the complexes to milder values by about 125 mV going from **1** to **3** or from **1a** to **3a**. Increasing the number of phosphane ligands has the opposite effect, lowering the reduction potential by about 180–200 mV per phosphane ligand. Pyridyl protonation also has a large effect on the electronics of the complexes, effectively counterbalancing the increase in electron density caused by phosphane substitution. Protonation of the pyridyl ligands of the mono-phosphane derivatives **1a**–**3a** has the effect of shifting the average CO frequency by about 11 wavenumbers to higher values while for the bis-phosphane complexes **1b** and **3b**, the average shift for the CO bands is roughly doubled at 20 cm^{-1}.

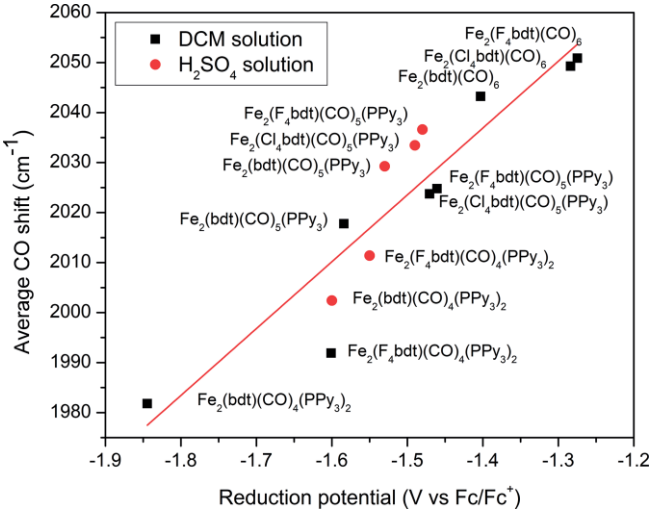

Figure 13. Plot of the average CO shift against the reduction potential of the complexes. In black are shown the data obtained in DCM solution while in red data obtained in diluted sulfuric acid solution.

The electron-withdrawing character of the bridge has a clear effect for the overpotential; complexes with electron-deficient di-iron cores display a milder first reduction potential and require milder catalytic potentials, but at the expense of lower proton reduction rates. In fact, moving from **1a** to **3a** the overpotential drops by about 100 mV while the catalytic activity decreases by roughly 30 % as the di-iron core of the complex becomes more electron-deficient. Similar values are observed moving from **1b** to **3b.**

In contrast to the behavior of the redox-active and proton-responsive dipyridylphosphole complex, the trispyridylphosphane complexes **1a**–**3a** do not show a PCET step in their mechanism when catalysis is performed in DCM solution in the presence of weak acid. Furthermore, the trispyridylphosphane ligand is purely acting as a spectator, remaining in its neutral form over the entire catalytic cycle. As such, the trispyridylphosphane does not play a beneficial role as proton-responsive ligand and it also increases the operational overpotential of the complexes by roughly 100 mV compared to the respective more electron-deficient hexacarbonyl parent complexes **1**. Interestingly, although the trispyridyl complexes are lacking any redox-active and proton-responsive properties, they require a significantly milder overpotential compared to the dipyridylphosphole complex previously reported.[24] The importance of the redox-active ligand is evidenced by the roughly 200 times higher catalytic rate of the dipyridylphosphole complex compared to the trispyridyl complexes. Upon reduction, the redox-activity of the dipyridylphosphole ligand allows for delocalization of some electron density onto the phosphorus-based ligand itself, therefore increasing the basicity of the pyridyl moieties. The increased basicity of the pyridyl groups in this phosphole ligand allows for their protonation and therefore proton preorganization around the di-iron center. This process happens in a concerted PCET fashion.[33] Figure 14 provides a visual comparison of the catalytic performances of the different complexes in DCM solution in the presence of weak acid. Undoubtedly such type of Tafel plots offer a clear and quick way to compare different catalysts, however, we stress that they are built from a single data point; the inflection point obtained by foot-of-the-wave analysis of the voltammograms. To build working comparative plots, more data points should be measured through preparative electrolysis experiments at different overpotentials.[62,65,66]

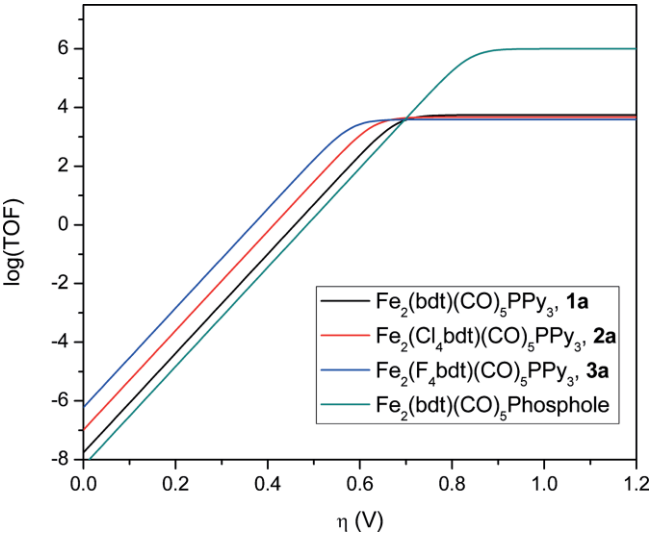

Figure 14. Tafel plot for complexes **1a**–**3a** in the presence of weak acid ($HNEt_3PF_6$), in DCM and comparison with reported values for the pyridyl phosphole derivative. The value of TOF_{max} is extrapolated for a 1 M concentration of substrate.

By comparing **1a** to **1b**, in DCM solution, it is clear that the coordination of a second phosphane ligand has a significant effect on the catalysis. The second phosphane makes the complex more electron-rich, which therefore requires about 200 mV higher overpotential to start the proton reduction reaction while the catalytic rates are only marginally higher. Although this complex shows an initial PCET step with weak acid, catalysis takes place at the more cathodic values of the second reduction. The pyridyl ligands, once more, do not partake in the catalytic mechanism nor do they preorganize the protons. A similar observation can be made when comparing **3a** to **3b**.

In diluted sulfuric acid, pyridyl protonation has the beneficial effect of lowering the electron-donating abilities of the phosphane ligands. As electron transfer steps are facilitated because of positive charges of the complexes, proton reduction happens at the first reduction. The presence of the pyridyl moieties and their inherent protonation in acidic aqueous solutions results in preorganization of the protons proximal to the catalytic di-iron center, likely to be the reason for the drastic increases in the activity of the complexes. For the mono-phosphane **1a**, going from organic solvent solution to acidic water has the effect of increasing the activity of the catalyst by four orders of magnitude, but at the expense of a significantly higher overpotential of about 140 mV. Figure 15 illustrates on the other hand that the bis-phosphane complex **1b** shows about five orders of magnitude higher activity in sulfuric acid than in organic solvents while the overpotential increases by a mere 30 mV as result of the higher number of active proton relays present on the complex. For the redox active phosphole derivative in acidic water media the overpotential drops by roughly 300 mV as result of the PCET step while its activity is only marginally increased as fewer proton relays are present on the ligand. These experiments show that proton preorganization via the pyridyl groups of the ligands plays a crucial role for boosting the catalytic rates in acidic water. The catalysts described in this contribution show remarkable activity for electrocatalytic hydrogen evolution with maximum turnover frequencies (TOF_{max}) in the order of 1.8×10^7 s^{-1} for **1a** and 2.7×10^8 s^{-1} for **1b**. To the best of our knowledge, such catalysts are among the fastest electrocatalysts reported in literature.[67]

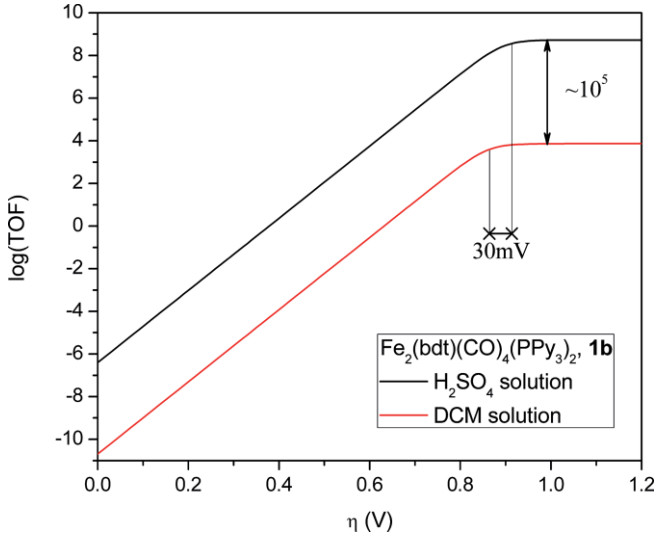

Figure 15. Tafel plot for complex **1b** in DCM solution in the presence of weak acid and in 0.5 M H_2SO_4 solution. TOF_{max} are extrapolated for a 1 M concentration of substrate.

Conclusions

We prepared and analyzed a series of the benzenedithiolate iron-iron hydrogenase models, with various numbers of P(*m*-Py)$_3$ ligands in order to understand the role of the pyridyl groups in proton reduction catalysis, also in relation to the recently reported analogue with a redox active phosphole-pyridyl ligand. Increasing the electron-withdrawing properties of the benzenedithiolate bridge leads to strongly electron-deficient di-iron cores, which, as a consequence, have lower catalytic proton reduction potentials while the decrease in their activity is modest. Complexes with phosphorus ligands coordinated have less favorable reduction potentials, but protonation of the pyridyl groups partially counterbalances the electron donating nature of the ligands. These pyridyl containing complexes are well soluble in acidic aqueous environment by protonation, and proton preorganization is suggested to increases the activity of the complex by a factor of five, while the increase in overpotential is negligible. Compared to the complex with the redox active phosphole ligand, which was studied under similar conditions in acidic water, the current complexes based on P(*m*-Py)$_3$ show much higher activity. The overpotential is also increased as the phosphane complexes appear to lack redox active properties that allow for PCET steps. This work therefore demonstrates that the presence of a proton-responsive ligand, which facilitates PCET, is important to lower the first reduction of the complexes, and when catalysis takes place at first reduction it effectively lowers the catalytic overpotential. These findings are relevant for further design and optimization of hydrogenase mimics for proton reduction catalysis.

Experimental Section

General procedures: all synthetic procedures were carried out under an argon atmosphere using standard Schlenk techniques. All commercially available chemicals were used as received without further purification. Solvents used for synthesis were dried, distilled and degassed with the most suitable method. Column chromatography was performed open to air using solvents as received.

Electrochemistry

Cyclic voltammetry was performed on 1 mM solution of analyte (unless otherwise stated) using 0.1 M tetrabutylammonium hexafluorophosphate as supporting electrolyte. The voltammograms were recorded using a PG-STAT302N potentiostat at glassy carbon disk electrode (2 mm diameter). A platinum coil was used as auxiliary electrode and a leak free silver electrode (inner compartment 3 M KCl/Ag) as reference electrode.

Spectroelectrochemistry was performed in an optically transparent thin layer OTTLE cell with platinum working electrode, platinum auxiliary electrode and silver wire as reference electrode, using 0.2 M tetrabutylammonium hexafluorophosphate as supporting electrolyte.

General Procedure for the Preparation of the hexacarbonyl complexes 1–3

An oven-dried, argon-flushed round-bottomed Schlenk flask equipped with a reflux condenser was charged with $Fe_3(CO)_{12}$ (4 mmol) and the dithiol precursor (1 equiv., 4 mmol). After addition of 200 mL of toluene, the reaction mixture was heated to 80 °C overnight in the dark. The reaction was cooled to room temperature and filtered through a plug of Celite before removing the volatiles under reduced pressure. The residue was dissolved in hexanes and chromatographed on silica gel to afford the clean compound.

Fe_2(bdt)$(CO)_6$, 1: 1.09 g, yield 65 %. ^{1}H NMR (CD_2Cl_2, ppm) δ 7.22 (dd, *J* = 5.7, 3.2 Hz, 2H), 6.71 (dd, *J* = 5.7, 3.2 Hz, 2H). ^{13}C NMR (CD_2Cl_2, ppm) δ 207.68, 147.46, 127.97, 126.79. FT-IR (hexane, ν) 2006, 2044, 2079 cm^{-1}.

Fe_2(Cl_4bdt)$(CO)_6$, 2: 0.89 g, Yield 40 %. ^{13}C NMR (CD_2Cl_2, ppm) δ 209.19, 206.61, 148.49, 131.49, 131.29, 129.29, 127.14. FT-IR (hexane, ν) 2014, 2050, 2084 cm^{-1}. **HR FD-MS** (*m*/*z*) found: 557.6581 expected: 557.6562, $C_{12}Cl_4Fe_2O_6S_2$.

Fe_2(F_4bdt)$(CO)_6$, 3: 1.24 g, yield 63 %. ^{13}C NMR (CD_2Cl_2, ppm) δ 209.19, 206.45, 151.09–146.59 (m), 145.59–143.37 (m), 141.77–139.46 (m), 138.04–136.10 (m), 133.48–130.54 (m). ^{19}F NMR (CD_2Cl_2, ppm) δ –131.05 (d, *J* = 20.0 Hz), –153.43 (d, *J* = 20.0 Hz). FT-IR (hexane, ν) 2015, 2052, 2086 cm^{-1}. HR FD-MS (*m*/*z*) found: 491.7750 expected: 491.7772, $C_{12}F_4Fe_2O_6S_2$

General Procedure for the Preparation of the mono-trispyridyl phosphane complexes 1a–3a

An oven-dried, argon-flushed round-bottomed Schlenk flask was charged with the hexacarbonyl complex **1–3** (0.6 mmol), trispyridyl phosphane (1 equiv., 0.6 mmol), and dichloromethane 60 mL. In a separate flask Me_3NO (1.5 equiv., 0.9 mmol) was dissolved in 2 mL of acetonitrile, and this solution was added to the first flask. After stirring the reaction mixture for 30 minutes at room temperature, in the dark the solvents were removed under reduced pressure. The residue was dissolved in minimal amount of DCM and chromatographed over silica gel with DCM/MeOH, 94:6 to afford the clean compound.

Fe_2(bdt)$(CO)_5$$PPy_3$, 1a: 299 mg, yield 76 %. ^{1}H NMR (CD_2Cl_2, ppm) δ 8.76–8.64 (m, 6H), 7.87 (t, *J* = 9.4, 3H), 7.38 (t, *J* = 6.4 Hz, 3H), 6.63 (dd, *J* = 5.5, 3.2 Hz, 2H), 6.32 (dd, *J* = 5.5, 3.2 Hz, 2H). ^{31}P NMR (CD_2Cl_2, ppm) δ 49.32. ^{13}C NMR (CD_2Cl_2, ppm) δ 212.83, 212.75, 208.66, 153.02, 152.86, 151.38, 147.24, 140.27, 140.13, 130.40, 129.91, 127.71, 125.94, 123.72, 123.63. FT-IR (hexane, ν) 1992, 2003, 2059 cm^{-1}. ^{1}H NMR (1 M D_2SO_4, ppm) δ 8.82–8.50 (m, 12H), 7.99 (t, *J* = 7.1 Hz, 3H), 6.44 (dd, *J* = 5.1, 3.0 Hz, 2H), 6.18 (dd, *J* = 5.1, 3.0 Hz, 2H). ^{31}P NMR (1 M D_2SO_4, ppm) δ 57.64. DOSY (1 M D_2SO_4) log D = –9.461 m^2 s^{-1}. FT-IR (1 M H_2SO_4, ν) 2015, 2005, 2069 cm^{-1}. HR FD-MS (*m*/*z*) found: 657.9080 expected: 657.9047, $C_{26}H_{16}Fe_2N_3O_5PS_2$.

Fe_2(Cl_4bdt)$(CO)_5$$PPy_3$, 2a: 233 mg, Yield 49 %. ^{1}H NMR (CD_2Cl_2, ppm) δ 8.75–8.59 (m, 6H), 7.95 (t, *J* = 9.6 Hz, 3H), 7.46 (m, 3H). ^{31}P NMR (CD_2Cl_2, ppm) δ 48.01. ^{13}C NMR (CD_2Cl_2, ppm) δ 212.13, 207.69, 152.84, 152.68, 151.79, 148.39, 140.28, 140.13, 131.18, 130.25, 129.70, 129.20, 123.91. FT-IR (hexane, ν) 1999, 2009, 2063 cm^{-1}. ^{1}H NMR (1 M D_2SO_4, ppm) δ 8.51 (d, *J* = 5.7 Hz, 3H), 8.48–8.37 (d, *J* = 6.3 Hz 3H), 8.25 (t, *J* = 9.4 Hz, 3H), 7.84–7.60 (m, 3H). ^{31}P NMR (1 M D_2SO_4, ppm) δ 55.88. DOSY(1 M D_2SO_4) log D = -9.739 m^2 s^{-1}. FT-IR (1 M H_2SO_4, ν) 2019, 2008 2073 cm^{-1}. HR FD-MS (*m*/*z*) found: 795.7462 expected: 795.7445, $C_{26}H_{12}Cl_4Fe_2N_3O_5PS_2$.

Fe_2(F_4bdt)$(CO)_5$$PPy_3$, 3a: 328 mg, yield 75 %. ^{1}H NMR (CD_2Cl_2, ppm) δ 8.96–8.56 (m, 6H), 7.97 (t, *J* = 10.0 Hz, 3H), 7.49 (m, 3H). ^{31}P NMR (CD_2Cl_2, ppm) δ 47.64. ^{13}C NMR (CD_2Cl_2, ppm) δ 211.98, 211.90, 207.53, 152.72, 151.87, 147.20, 143.83, 140.29, 140.14, 131.55, 129.73, 129.21, 124.00. ^{19}F NMR (CD_2Cl_2, ppm) δ –131.16 (d, *J* = 19.5 Hz), –154.99 (d, *J* = 19.5 Hz). FT-IR (hexane, ν) 2000, 2010, 2065 cm^{-1}. ^{1}H NMR (1 M D_2SO_4, ppm) δ 8.51 (m, 6H), 8.33 (t, *J* = 9.3 Hz, 3H), 7.74 (m, 3H). ^{31}P NMR (1 M D_2SO_4, ppm) δ 54.94. ^{19}F NMR (1 M D_2SO_4, ppm) δ –128.02 (d, *J* = 20.1 Hz), –150.72 (d, *J* = 20.1 Hz). DOSY(1 M D_2SO_4) log D = –9.476 m^2 s^{-1}. FT-IR (1 M H_2SO_4, ν) 2023, 2012, 2075 cm^{-1}. HR FD-MS (*m*/*z*) found: 729.8697 expected: 729.8670, $C_{26}H_{12}F_4Fe_2N_3O_5PS_2$.

General Procedure for the Preparation of the bis-trispyridyl phosphane complexes 1b and 3b

An oven-dried, argon-flushed round-bottomed Schlenk flask was charged with the hexacarbonyl complex **1** or **3** (0.3 mmol), trispyridyl phosphane (2.5 molar equiv., 0.75 mmol) and toluene (60 mL). The reaction mixture was refluxed for 2 hours. After cooling the reaction mixture to room temperature, the volatiles were removed under reduced pressure. The residue was dissolved in dichloromethane and the complexes precipitated with hexanes. After three recrystallizations the solids were washed with hexanes before drying under vacuum.

Fe_2(bdt)$(CO)_4$$(PPy_3)_2$, 1b: 233 mg, yield 87 %. ^{1}H NMR (CD_2Cl_2, ppm) δ 8.64 (m, 12H), 7.85(t, *J* = 9.2 Hz, 6H), 7.34 (dd, *J* = 7.9, 4.8 Hz, 6H), 6.02 (dd, *J* = 5.4, 3.2 Hz, 2H), 5.91 (dd, *J* = 5.4, 3.2 Hz, 2H). ^{31}P NMR (CD_2Cl_2, ppm) δ 46.57. ^{13}C NMR (CD_2Cl_2, ppm) δ 214.04, 214.00, 213.96, 152.86, 152.80, 152.73, 150.94, 146.84, 140.16, 140.11, 140.05, 130.53, 130.17, 127.47, 124.97, 123.47, 123.41. FT-IR (DCM, ν) 1950, 1966, 2010 cm^{-1}. ^{1}H NMR (1 M D_2SO_4, ppm) δ 8.73 (d, *J* = 5.8 Hz, 6H), 8.71–8.52 (m, 12H), 7.99 (t, *J* = 7.1 Hz, 6H), 6.20–5.61 (m, 4H). ^{31}P NMR (1 M D_2SO_4, ppm) δ 56.18. DOSY(1 M D_2SO_4) log D = –9.482 m^2 s^{-1}. FT-IR (1 M H_2SO_4, ν) 1982, 1992 2033 cm^{-1}. HR FD-MS (*m*/*z*) found: 893.9783 expected: 893.9789, $C_{40}H_{28}Fe_2N_6O_4P_2S_2$.

Fe_2(F_4bdt)$(CO)_4$$(PPy_3)_2$, 3b: 237 mg, yield 82 %. ^{1}H NMR (CD_2Cl_2, ppm) δ 8.68 (m, 12H), 7.94 (t, *J* = 9.2 Hz, 6H), 7.43 (m, 6H). ^{31}P NMR (CD_2Cl_2, ppm) δ 44.94. ^{19}F NMR (CD_2Cl_2, ppm) δ –131.13 (d, *J* = 19.9 Hz), –156.52 (d, *J* = 19.9 Hz). ^{13}C NMR (CD_2Cl_2, ppm) δ 213.32, 213.26, 152.73, 151.57, 147.41, 140.29, 140.15, 131.38, 130.03, 129.58, 123.84. FT-IR (DCM, ν) 1960, 1976, 2018 cm^{-1}. ^{1}H NMR (1 M D_2SO_4, ppm) δ 8.85 (d, *J* = 5.0 Hz, 6H), 8.81 (d, *J* = 5.6 Hz, 6H), 8.62 (t, *J* = 8.6 Hz, 6H), 8.02 (t, *J* = 7.1 Hz, 6H). ^{31}P NMR (1 M D_2SO_4, ppm) δ 53.54. ^{19}F NMR (1 M D_2SO_4, ppm) δ –128.73 (d, *J* = 18.5 Hz), –151.60 (d, *J* = 18.5 Hz). DOSY(1 M D_2SO_4) log D = –9.491 m^2 s^{-1}. FT-IR (1 M H_2SO_4, ν) 1992, 2001, 2041 cm^{-1}. HR FD-MS (*m*/*z*) found: 965.9458 expected: 965.9412, $C_{40}H_{24}F_4Fe_2N_6O_4P_2S_2$.

CCDC 1848258 (for **3**), 1848256 (for **1a**), 1848257 (for **2a**), 1848259 (for **3a**), and 1848260 (for **1b**) contain the supplementary crystallographic data for this paper. These data can be obtained free of charge from The Cambridge Crystallographic Data Centre.

Acknowledgments

This work is part of the research program of the Foundation for Fundamental Research on Matter (FOM), which is part of the Netherlands Organisation for Scientific Research (NWO). We thank L. Jongkind for the synthesis of tris(*m*-pyridyl)phosphane and E. Zuidinga for mass analysis.

Keywords: [FeFe]-Hydrogenase mimics · Proton relays · Phosphane ligands · Homogeneous catalysis · Hydrogen evolution

[1] M. Frey, *ChemBioChem* **2002**, *3*, 153–160.
[2] J. C. Fontecilla-Camps, A. Volbeda, C. Cavazza, Y. Nicolet, *Chem. Rev.* **2007**, *107*, 4273–4303.
[3] S. E. McGlynn, D. W. Mulder, E. M. Shepard, J. B. Broderick, J. W. Peters, *Dalton Trans.* **2009**, 4274–4285.
[4] J. W. Peters, G. J. Schut, E. S. Boyd, D. W. Mulder, E. M. Shepard, J. B. Broderick, P. W. King, M. W. Adams, *Biochim. Biophys. Acta Mol. Cell Res.* **2015**, *1853*, 1350–1369.
[5] F. A. Armstrong, N. A. Belsey, J. A. Cracknell, G. Goldet, A. Parkin, E. Reisner, K. A. Vincent, A. F. Wait, *Chem. Soc. Rev.* **2009**, *38*, 36–51.
[6] M. Wang, L. Chen, L. C. Sun, *Energy Environ. Sci.* **2012**, *5*, 6763–6778.
[7] W. Lubitz, H. Ogata, O. Rudiger, E. Reijerse, *Chem. Rev.* **2014**, *114*, 4081–4148.
[8] C. Sommer, A. Adamska-Venkatesh, K. Pawlak, J. A. Birrell, O. Rudiger, E. J. Reijerse, W. Lubitz, *J. Am. Chem. Soc.* **2017**, *139*, 1440–1443.
[9] H. Li, T. B. Rauchfuss, *J. Am. Chem. Soc.* **2002**, *124*, 726–727.
[10] T. B. Rauchfuss, *Acc. Chem. Res.* **2015**, *48*, 2107–2116.
[11] D. Schilter, T. B. Rauchfuss, *Angew. Chem. Int. Ed.* **2013**, *52*, 13518–13520; *Angew. Chem.* **2013**, *125*, 13760.
[12] S. Ezzaher, A. Gogoll, C. Bruhn, S. Ott, *Chem. Commun.* **2010**, *46*, 5775–5777.
[13] S. Ezzaher, P. Y. Orain, J. F. Capon, F. Gloaguen, F. Y. Petillon, T. Roisnel, P. Schollhammer, J. Talarmin, *Chem. Commun.* **2008**, 2547–2549.
[14] J.-F. Capon, S. Ezzaher, F. Gloaguen, F. Y. Pétillon, P. Schollhammer, J. Talarmin, *Chem. Eur. J.* **2008**, *14*, 1954–1964.
[15] T. Liu, M. Wang, Z. Shi, H. Cui, W. Dong, J. Chen, B. Åkermark, L. Sun, *Chem. Eur. J.* **2004**, *10*, 4474–4479.
[16] C. Esmieu, G. Berggren, *Dalton Trans.* **2016**, *45*, 19242–19248.
[17] L.-C. Song, L.-X. Wang, B.-S. Yin, Y.-L. Li, X.-G. Zhang, Y.-W. Zhang, X. Luo, Q.-M. Hu, *Eur. J. Inorg. Chem.* **2008**, *2008*, 291–297.
[18] M. Bourrez, R. Steinmetz, F. Gloaguen, *Inorg. Chem.* **2014**, *53*, 10667–10673.
[19] S. Ezzaher, J.-F. Capon, F. Gloaguen, F. Y. Pétillon, P. Schollhammer, J. Talarmin, N. Kervarec, *Inorg. Chem.* **2009**, *48*, 2–4.
[20] L. Duan, M. Wang, P. Li, N. Wang, F. Wang, L. Sun, *Inorg. Chim. Acta* **2009**, *362*, 372–376.
[21] Z. Wang, J. Liu, C. He, S. Jiang, B. Åkermark, L. Sun, *Inorg. Chim. Acta* **2007**, *360*, 2411–2419.
[22] Z. Wang, J.-H. Liu, C.-J. He, S. Jiang, B. Åkermark, L.-C. Sun, *J. Organomet. Chem.* **2007**, *692*, 5501–5507.
[23] J. Chen, A. K. Vannucci, C. A. Mebi, N. Okumura, S. C. Borowski, M. Swenson, L. T. Lockett, D. H. Evans, R. S. Glass, D. L. Lichtenberger, *Organometallics* **2010**, *29*, 5330–5340.
[24] Y. Wang, M. Wang, L. Sun, M. S. G. Ahlquist, *Chem. Commun.* **2012**, *48*, 4450–4452.
[25] N. Wang, M. Wang, Y. Wang, D. Zheng, H. Han, M. S. G. Ahlquist, L. Sun, *J. Am. Chem. Soc.* **2013**, *135*, 13688–13691.
[26] M. L. Helm, M. P. Stewart, R. M. Bullock, M. R. DuBois, D. L. DuBois, *Science* **2011**, *333*, 863–866.
[27] J. Y. Yang, R. M. Bullock, M. R. DuBois, D. L. DuBois, *MRS Bull.* **2011**, *36*, 39–47.
[28] D. L. DuBois, *Inorg. Chem.* **2014**, *53*, 3935–3960.
[29] M. Rakowski DuBois, D. L. DuBois, *Chem. Soc. Rev.* **2009**, *38*, 62–72.
[30] N. Wang, M. Wang, T. Zhang, P. Li, J. Liu, L. Sun, *Chem. Commun.* **2008**, 5800–5802.
[31] D. H. Pool, M. P. Stewart, M. O'Hagan, W. J. Shaw, J. A. S. Roberts, R. M. Bullock, D. L. DuBois, *Proc. Natl. Acad. Sci. USA* **2012**, *109*, 15634–15639.
[32] R. M. Henry, R. K. Shoemaker, D. L. DuBois, M. R. DuBois, *J. Am. Chem. Soc.* **2006**, *128*, 3002–3010.
[33] R. Becker, S. Amirjalayer, P. Li, S. Woutersen, J. N. Reek, *Sci. Adv.* **2016**, *2*, e1501014.
[34] D. Schilter, J. M. Camara, M. T. Huynh, S. Hammes-Schiffer, T. B. Rauchfuss, *Chem. Rev.* **2016**, *116*, 8693–8749.
[35] J. C. Lansing, J. M. Camara, D. E. Gray, T. B. Rauchfuss, *Organometallics* **2014**, *33*, 5897–5906.
[36] J. M. Camara, T. B. Rauchfuss, *Nat. Chem.* **2012**, *4*, 26–30.
[37] C. Tard, X. Liu, S. K. Ibrahim, M. Bruschi, L. D. Gioia, S. C. Davies, X. Yang, L.-S. Wang, G. Sawers, C. J. Pickett, *Nature* **2005**, *433*, 610–613.
[38] M. L. Singleton, D. J. Crouthers, R. P. Duttweiler, J. H. Reibenspies, M. Y. Darensbourg, *Inorg. Chem.* **2011**, *50*, 5015–5026.
[39] R. Mejia-Rodriguez, D. Chong, J. H. Reibenspies, M. P. Soriaga, M. Y. Darensbourg, *J. Am. Chem. Soc.* **2004**, *126*, 12004–12014.
[40] Y. Na, M. Wang, K. Jin, R. Zhang, L. Sun, *J. Organomet. Chem.* **2006**, *691*, 5045–5051.
[41] W. N. Cao, F. Wang, H. Y. Wang, B. Chen, K. Feng, C. H. Tung, L. Z. Wu, *Chem. Commun.* **2012**, *48*, 8081–8083.
[42] F. Quentel, G. Passard, F. Gloaguen, *Chem. Eur. J.* **2012**, *18*, 13473–13479.
[43] F. Quentel, G. Passard, F. Gloaguen, *Phys. Chem. Chem. Phys.* **2012**, *5*, 7757–7761.
[44] M. J. Baker-Hawkes, E. Billig, H. B. Gray, *J. Am. Chem. Soc.* **1966**, *88*, 4870–4875.
[45] E. J. Wharton, J. A. McCleverty, *J. Chem. Soc. A* **1969**, 2258–2266.
[46] A. H. Hoveyda, R. K. M. Khan, S. Torker, M. J. Koh, *PCT Int. Appl. (**2014**), WO2014201300*.
[47] J. A. Cabeza, M. A. Martínez-García, V. Riera, D. Ardura, S. García-Granda, *Organometallics* **1998**, *17*, 1471–1477.
[48] E. S. Donovan, J. J. McCormick, G. S. Nichol, G. A. N. Felton, *Organometallics* **2012**, *31*, 8067–8070.
[49] L. Schwartz, P. S. Singh, L. Eriksson, R. Lomoth, S. Ott, *C. R. Chim.* **2008**, *11*, 875–889.
[50] I. K. Pandey, S. M. Mobin, N. Deibel, B. Sarkar, S. Kaur-Ghumaan, *Eur. J. Inorg. Chem.* **2015**, *2015*, 2875–2882.
[51] A. K. Vannucci, S. Wang, G. S. Nichol, D. L. Lichtenberger, D. H. Evans, R. S. Glass, *Dalton Trans.* **2010**, *39*, 3050–3056.
[52] G. A. N. Felton, A. K. Vannucci, J. Chen, L. T. Lockett, N. Okumura, B. J. Petro, U. I. Zakai, D. H. Evans, R. S. Glass, D. L. Lichtenberger, *J. Am. Chem. Soc.* **2007**, *129*, 12521–12530.
[53] J.-F. Capon, F. Gloaguen, P. Schollhammer, J. Talarmin, *J. Electroanal. Chem.* **2006**, *595*, 47–52.
[54] J.-F. Capon, F. Gloaguen, P. Schollhammer, J. Talarmin, *J. Electroanal. Chem.* **2004**, *566*, 241–247.
[55] H. J. Paul, J. Leddy, *Anal. Chem.* **1995**, *67*, 1661–1668.
[56] C. L. Bentley, A. M. Bond, A. F. Hollenkamp, P. J. Mahon, J. Zhang, *Anal. Chem.* **2014**, *86*, 2073–2081.
[57] T.-H. Yen, K.-T. Chu, W.-W. Chiu, Y.-C. Chien, G.-H. Lee, M.-H. Chiang, *Polyhedron* **2013**, *64*, 247–254.
[58] S. Derossi, R. Becker, P. Li, F. Hartl, J. N. H. Reek, *Dalton Trans.* **2014**, *43*, 8363–8367.
[59] A. M. Kluwer, R. Kapre, F. Hartl, M. Lutz, A. L. Spek, A. M. Brouwer, P. W. N. M. van Leeuwen, J. N. H. Reek, *Proc. Natl. Acad. Sci. USA* **2009**, *106*, 10460–10465.
[60] A. Darchen, H. Mousser, H. Patin, *J. Chem. Soc., Chem. Commun.* **1988**, 968–970.
[61] F. Gloaguen, D. Morvan, J.-F. Capon, P. Schollhammer, J. Talarmin, *J. Electroanal. Chem.* **2007**, *603*, 15–20.
[62] C. Costentin, S. Drouet, M. Robert, J. M. Saveant, *J. Am. Chem. Soc.* **2012**, *134*, 11235–11242.
[63] C. Costentin, *Chem. Rev.* **2008**, *108*, 2145–2179.
[64] C. Costentin, M. Robert, J.-M. Savéant, *J. Electroanal. Chem.* **2006**, *588*, 197–206.
[65] C. Costentin, M. Robert, J. M. Saveant, *Chem. Soc. Rev.* **2013**, *42*, 2423–2436.
[66] V. Artero, J.-M. Saveant, *Energy Environ. Sci.* **2014**, *7*, 3808–3814.
[67] A. J. P. Cardenas, B. Ginovska, N. Kumar, J. Hou, S. Raugei, M. L. Helm, A. M. Appel, R. M. Bullock, M. O'Hagan, *Angew. Chem. Int. Ed.* **2016**, *55*, 13509–13513; *Angew. Chem.* **2016**, *128*, 13707.

Received: January 19, 2019